PAPER • OPEN ACCESS

Ultra-giant magnetoresistance in graphene-based spin valves with gate-controlled potential barriers

New Journal of Physics
The open access journal at the forefront of physics

Deutsche Physikalische Gesellschaft DPG
IOP Institute of Physics

Published in partnership with: Deutsche Physikalische Gesellschaft and the Institute of Physics

OPEN ACCESS

RECEIVED
29 May 2019

REVISED
29 October 2019

ACCEPTED FOR PUBLICATION
31 October 2019

PUBLISHED
18 November 2019

PAPER

Ultra-giant magnetoresistance in graphene-based spin valves with gate-controlled potential barriers

Peng Tseng and Wen-Jeng Hsueh

Nanomagnetism Group, Department of Engineering Science and Ocean Engineering, National Taiwan University, 1, section 4, Roosevelt Road, Taipei, 10617, Taiwan

E-mail: hsuehwj@ntu.edu.tw

Keywords: spintronics, giant magnetoresistance, graphene spin transport, spin valve, graphene nanoribbons

Abstract

Pursuing larger tunnel magnetoresistance is a significant work to develop attractive spin-valve devices for high-performance read heads of hard disk drives, magnetic random access memories, and transistors. Here, we propose an ultra-giant magnetoresistance reaching higher than 40 000% at room temperature by using a spin valve of an armchair graphene nanoribbon with double gate-controlled potential barriers. The ultra-giant magnetoresistance approximately 60 times larger than that of traditional MgO-barrier spin valves is caused by an extraordinary current suppression in the antiparallel mode. Moreover, owing to the concept of the gate-voltage barrier, the proposed system provided not only lower complexity of the fabricating standard but also longer endurance of the operation than traditional spin-valve devices.

1. Introduction

Magnetoresistive effect in spin-valve devices has attracted considerable attention in the emerging field of spintronics because of its unique physical mechanism and magnetic properties [1–5]. Spin-valve devices have been recognized to be applicable in magnetic field-effect transistors [1, 6], magnetic sensors [7], read heads of hard disk drives [7, 8], and magnetic random access memories [4, 9, 10]. In general, the main structure of a typical spin valve contains a magnetic tunnel junction (MTJ), which consists of two ferromagnetic materials and an insulator as the middle spacer (F/I/F). In the past few years, several researchers have proposed that utilizing crystalline insulators, i.e. magnesium oxide (MgO), to replace the amorphous aluminum oxide can improve the tunnel magnetoresistance (TMR) ratio from 70% to 180% at room temperature [9]. Remarkably, considering the strict orientation of the MgO (001) barrier between the boundaries of the CoFeB compositions and the tantalum layers, a high room-temperature TMR ratio of up to 604% at 300 K and 1144% at 5 K was obtained in such MTJ storage cells [11]. A superlattice MTJ tried to approach a large TMR at an extremely low temperature [5]. However, more high-precision fabrication technologies are required for the production of such nanoscale multilayers. In addition, the degradation of the MgO barrier is another critical disadvantage that reduces device lifetime [12]. More recently, given the complex and strict manufacturing process of the excellent MgO barrier, several studies have successfully attempted the use of different insulating materials, such as hexagonal boron nitride (h-BN) [13], non-magnetic nanoparticles [7], and molybdenum disulfide (MoS_2) [14], as the tunneling barrier in MTJs with the expectation of simplification and structural stability, but the TMR ratios are lower than that of MgO-barrier MTJs.

Graphene, with its two-dimensional honeycomb lattice of carbon atoms, has been an attractive new class for its particular physical characteristics and promising applications in nanoelectronics and optoelectronics [15–17]. Edge states in graphene nanoribbons (GNRs) strongly affect the operation of magnetic transport [18–20]. In the state-of-the-art field, the exploration of spintronics in graphene-based devices has become increasingly popular [21–24]. Although previous studies have theoretically shown that lateral spin valves with GNRs reach extensive magnetoresistance (MR) at low temperatures [25, 26], the experiment results have reported the reduction of the MR magnitude in a similar structure to only 12% at room temperature [27, 28].

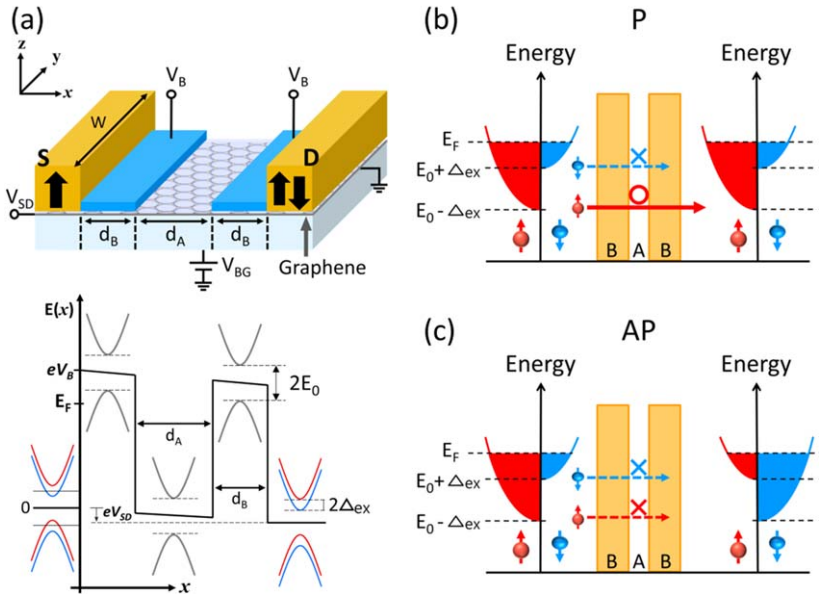

Figure 1. (a) Schematic representation of a lateral aGNR spin valve with double gate barriers. The blue electrodes represent the top gates that induce squared potential barriers V_B on aGNR. Potential profiles and dispersion relation in each section are shown in the lower sketch. Bandgap $2E_0$ at the Dirac cone based on the armchair edge state causes the nonlinear dispersions. The proximity-induced exchange splitting exerts on graphene, leading to the spin-up and spin-down states of dispersion. Schematic representations of the spin-dependent energy states for ferromagnetic electrodes in the (b) P and (c) AP configurations. The red and blue segments represent the energy states of the spin-up and spin-down electrons. The solid and dashed arrows indicate the allowed and prohibited transport of the spin-polarized electrons in the system, respectively.

Little investigation has been done with regard to the consistency between the theoretical and the experimental results at room temperature. Recent works have reported a new paradigm for GNR spin valves with an insulator barrier constructed by a two-dimensional material, such as h-BN. The structure is similar to that in typical MTJs with the MR value of less than 100% [29, 30]. However, the h-BN barrier devices suffer from roughness, defects, and fabrication issues. Moreover, the MR ratios of such devices are significantly lower than the MR ratio of a typical MgO-based MTJ. Hence, thus far, extensive research efforts have been aimed at achieving not only a lower fabricating standard and longer operating lifetime but also higher MR performance for the applications of graphene spintronic devices.

In this article, a room-temperature MR ratio of above 40 000% in an armchair graphene nanoribbon (aGNR) spin valve with gate-controlled potential barriers is proposed, which is approximately 60 and 400 times of the MR values in MTJs and aGNR spin valves, respectively. The ultra-giant MR is caused by a restrained current about a hundredth of the original in the antiparallel configuration, utilizing the manipulation of the transmission band. The proposed method is demonstrated by theoretical [31, 32] and experimental [27, 28] works. Compared with the high-quality MgO and traditional crystal insulators, this work adopts a more effective method to simplify the fabrication and enhance the endurance of the devices through the gate-controlled potential barriers [33–35].

2. Model and formulation

A double-barrier spin valve and a lateral aGNR as the electronic transport channel are considered, as shown in figure 1(a). The width of the aGNR is denoted as W. The top non-gated and gated segments in figure 1(a), denoted as A and B, respectively, indicate the non-magnetic aGNR of potential $V_A = 0$ with the distance between two barriers d_A and potential barriers V_B with thickness d_B. Tunable voltage gates can achieve the variations of potential barriers V_B and lengths, d_A and d_B. The left and right yellow-block segments denoted as source (S) and drain (D) electrodes, respectively, represent ferromagnetic insulators such as EuO that can induce magnetization vectors on the aGNR channel as two ferromagnetic aGNR (FG) electrodes. The black arrows indicate the magnetization of FG in either parallel (P) or antiparallel (AP) configurations along the z-direction, thereby forming an exchange splitting energy (Δ_{ex}) by proximity-induced effects [36, 37]. The applied transverse voltage between electrode S and electrode D, denoted as V_{SD}, is responsible for tunneling the current from the source to the drain. Note that the aGNR channel length of at least 5 nm is reserved to assure a sufficient transport region.

In a low-energy analysis of spin-dependent carriers near the K point, the two-dimensional Dirac Hamiltonian [15] can be expressed as follows:

$$\hat{H} = v_F \hat{\sigma} \cdot \hat{p} + U(x) - \zeta \Delta_{ex}, \tag{1}$$

where $v_F = \sqrt{3}\,at/2\hbar \approx 10^6$ m s^{-1} is the Fermi velocity, $\hat{\sigma} = (\sigma_x, \sigma_y, \sigma_z)$ denotes the Pauli matrix, $\hat{p} = (p_x, p_y, 0)$ is the in-plane momentum operator with two components, and $U(x)$ is the electrostatic potential. $\zeta = +\,(\zeta = -)$ denotes the spin-up (spin-down) index, and Δ_{ex} is the component of exchange splitting on the FG electrodes with the proximity-induced effect.

The solution to the two-dimensional Dirac equation $H\Psi = E\Psi$ is $\Psi_\rho = (\Psi_\rho^A, \Psi_\rho^B)^T$, where T is the transpose of the matrix, A and B are the sublattices of graphene, and $\rho = \uparrow,\downarrow$ denote the spin orientations. Due to the translational invariance along the y-direction, the wave function is written as $\Psi_\rho^{A(B)}(x, y) = \psi_\rho^{A(B)}(x)e^{ik_y y}$. Therefore, the details of the general solution to the above equation with spin components in the jth segment can be expressed as $\Psi_\rho^A = e^{ik_y y}(a_j^{\rho+}e^{iq_j^\rho \cdot x} + b_j^{\rho-}e^{-iq_j^\rho \cdot x})$ and $\Psi_\rho^B = e^{ik_y y}\left(\frac{q_j^\rho + ik_y}{k_j^\rho}a_j^{\rho+}e^{iq_j^\rho \cdot x} - \frac{q_j^\rho + ik_y}{k_j^\rho}b_j^{\rho-}e^{-iq_j^\rho \cdot x}\right)$, where $a_j^{\rho+}$ and $b_j^{\rho-}$ are the amplitude of the incident and reflected waves, respectively, and the total momentum is $k_j^\rho = (E - U_j + \zeta\Delta_{ex})$ with incident energy E. Noticeably, k_j^ρ is $E - U_j$ outside the S and D regions. Furthermore, $q_j^\rho = \mathrm{sgn}\,(k_j^\rho)\sqrt{(k_j^\rho)^2 - (k_y)^2}$ is the x component of the momentum for $(k_j^\rho)^2 > (k_y)^2$; otherwise, $q_j^\rho = i\sqrt{(k_y)^2 - (k_j^\rho)^2}$, and k_y is the y component of the momentum.

With the standard transfer-matrix method on each segment, the relation between the source and the drain electrodes can be connected with the total transfer matrix M, namely, $\begin{Bmatrix} a_D^{\rho+} \\ b_D^{\rho-} \end{Bmatrix} = M_{\rho\rho}\begin{Bmatrix} a_S^{\rho+} \\ b_S^{\rho-} \end{Bmatrix}$, where $M_{\rho\rho} = N_{D\rho}^{-1}(\prod_{j=1}^{n} C_{j\rho})N_{S\rho}$, $C_{j\rho} = H_{j\rho}N_{j\rho}^{-1}$, $H_{j\rho} = \begin{pmatrix} e^{iq_j^\rho \cdot d_j} & e^{-iq_j^\rho \cdot d_j} \\ (q_j^\rho + ik_y)e^{iq_j^\rho \cdot d_j}/k_j^\rho & -(q_j^\rho - ik_y)e^{-iq_j^\rho \cdot d_j}/k_j^\rho \end{pmatrix}$, $N_{j\rho} = \begin{pmatrix} 1 & 1 \\ (q_j^\rho + ik_y)/k_j^\rho & -(q_j^\rho - ik_y)/k_j^\rho \end{pmatrix}$, d_j is the length of each jth segment, and n is the total number of layers. The transmission of spin electrons passing through the entire system is given by $T_{\rho\rho}(E) = 1 - |m_{21}/m_{22}|^2$. According to the Landauer–Buttiker formalism [38], the spin-polarized currents for the spin-up or spin-down transport can be expressed as follows:

$$I_{SD}^{\rho\rho} = \frac{e}{h}\sum_m \int_{-\infty}^{\infty} T_{\rho\rho}[f_S(E - \mu_S) - f_D(E - \mu_D)]\,dE, \tag{2}$$

where $f_S = \{1 + \exp[(E - \mu_S)/k_BT]\}^{-1}$ and $f_D = \{1 + \exp[(E - \mu_D)/k_BT]\}^{-1}$ are the Fermi–Dirac distributions on the S and the D, respectively. μ_S and μ_D denote the chemical potentials of the S and the D, respectively, and the MR ratio is defined as $\mathrm{MR} = (I_P^{total} - I_{AP}^{total})/I_{AP}^{total}$, where $I_{P(AP)}^{total} = I_{P(AP)}^{\uparrow} + I_{P(AP)}^{\downarrow}$ is the total current. In the case of aGNRs, the quantized transverse momentum, denoted as $k_{y,m}$, is a unique property due to the boundary conditions of the GNR edge state. An aGNR can be metallic, $k_{y,m} = 0$, or semiconducting, $|k_y(m)| = m\pi/3W$, where $m = 1, 2, 4, 5, 7, \ldots \notin 3\mathbb{N}$ is an integer multiple of the lattice constant, as given in the [31]. W is the width of the aGNR. Therefore, the half-bandgap can be obtained as $E_0 = \hbar v_F k_y(1) = \hbar v_F \pi/3W$ with the first-order transverse momentum $\hbar k_y(1)$, and m is selected as 1.

3. Results and discussion

Figures 1(b) and (c) show the energy states of two FG electrodes in the double-barrier aGNR spin valve. Because of the edge state and exchange splitting, the origins of the energy states on both FG electrodes split into $E_0 - \Delta_{ex}$ ($E_0 + \Delta_{ex}$) for the spin-up (spin-down) electrons [37], where E_0 is the half-bandgap of the aGNR. The red and blue vertical arrows represent the spin-up and spin-down electrons, respectively. In traditional graphene-based spin valves, i.e. FG/NG/FG, the energy window between $E_0 - \Delta_{ex}$ ($E_0 + \Delta_{ex}$) and E_F of the spin-up (spin-down) electrons is always conductive in the P configuration because of the non-barrier spacer [25]. In the same manner, the energy windows of both types of spin-polarized electrons begin at $E_0 + \Delta_{ex}$ in the AP configuration, because there are no corresponding states before $E_0 + \Delta_{ex}$ on the drain electrode, as shown in figure 1(c). The conductive and non-conductive properties are able to be controlled in each energy range by combining different barriers in the middle spacer. The concept is similar to the band structure in periodic multilayers [5, 26, 39]. In this work, all the transport of the spin-polarized electrons between the energy window $E_0 + \Delta_{ex}$ and E_F can be designed to be forbidden by adjusting the double-barrier junction (see discussion in figure 4). However, the electron transport of the spin-up polarization presents an unobstructed penetration within the energy range, $E_0 - \Delta_{ex}$ to $E_0 + \Delta_{ex}$, only for the P configuration (discussion in figure 4(a)). This phenomenon can be related to the resonant tunneling by quantum-well states in the central spacer [10] and the

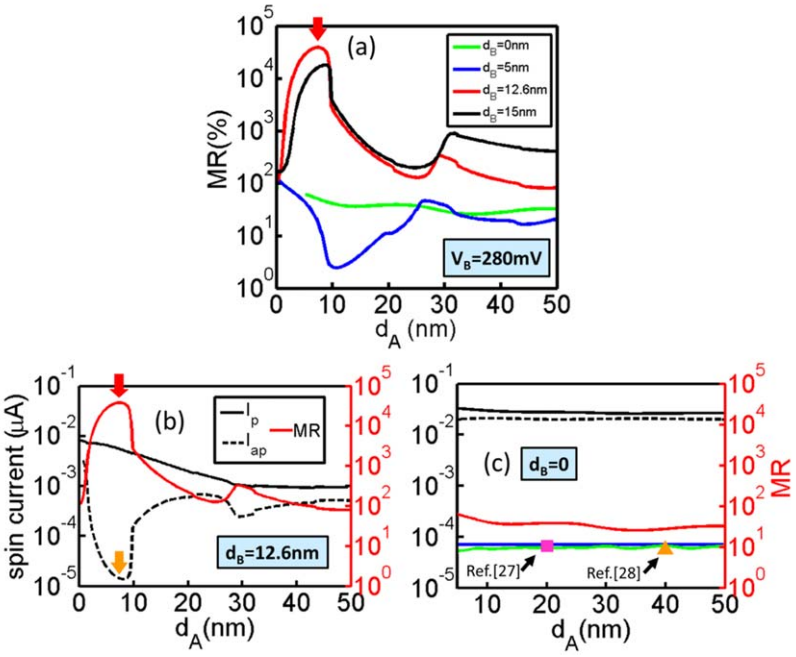

Figure 2. (a) Room-temperature MR ratio versus distance between two barriers d_A with $V_B = 280$ mV. (b) Spin-polarized current and MR ratio versus distance between two top gates d_A with fixed $d_B = 12.6$ nm. The red arrows indicate the MR peaks. (c) Spin-polarized current and MR ratio versus d_A with fixed $d_B = 0$ nm. The green and blue solid lines represent the corresponding MR ratio obtained by the proposed method when all of the parameters except d_A are considered in [27, 28], respectively. The rectangle and the triangle marks indicate the experimental results presented in [27, 28], respectively. The scales of d_A in the green and blue lines are 10 and 20 times as large as those on the original x-axis. The parameters of the system are $V_A = 0$ mV, $V_{SD} = 1$ mV, $\Delta_{ex} = 20$ meV, $\mu_D = 110.3$ meV, and $T = 300$ K.

difference in the spin splitting states. Thus, when the spin channel of transmission is designed within the energy window $[E_0 - \Delta_{ex}, E_0 + \Delta_{ex}]$, the transport of the spin-up electron is transmitted in the P configuration, as seen in figure 1(b). That is, the spin-up polarization predominates a high proportion in the P mode to maintain the major current flow. In contrast, because such an energy window is nonexistent in the AP configuration, both propagations of the spin-up and spin-down electrons are restricted in the AP mode, as illustrated in figure 1(c).

Figure 2(a) quantitatively shows the MR effect for altering the distance between two barriers d_A, where the others parameters are $V_A = 0$ mV, $V_B = 280$ mV, $V_{SD} = 1$ mV, $\Delta_{ex} = 20$ meV, chemical potential $\mu_D = E_0 = 110.3$ meV, $\mu_S = \mu_D + eV_{SD}$, and temperature $T = 300$ K. The figure shows that the maximum MR ratio exceeds 40 000% in the double-barrier structure with a d_A value of 7.5 nm and a d_B value of 12.6 nm, as indicated by the red curve in figures 2(a) and (b), respectively. The maximum MR peaks are indicated by the red arrows in figure 2. The system still maintains good operational efficiency with high MR ratios when a minor error occurs in the device size. The features of the spin-polarized current are clearly shown in figure 2(b) to explain the reason for the large MR ratio. In figure 2(b), the graph shows that the huge MR is induced by an extremely low current valley which is indicated by the yellow arrow. The spin-up current is almost insusceptible with the distance variation in the P configuration. The entire system is provided with a large resistance owing to the limited conduction of the electron penetration in the AP configuration. The result can be obtained with the constriction bands of spin-polarized electrons controlled by the double-barrier junction. In the P configuration, the resistance of the system modulates extremely little because of the resonance effect. The phenomenon of the MR change conforms to the standard requirement for typical spin-valve devices [9, 11]. However, to the best of our knowledge, high MR effects are usually determined by the enhancement of the P-mode tunneling current rather than the restraint of the AP-mode current in a traditional resonance system. The mechanism of the enhanced AP resistance to induce an ultra-giant MR effect is considerably rare compared with the mechanism of a typical double-barrier structure. This is the main reason for the giant MR value obtained in this study. A special case, figure 2(c) shows an ordinary MR ratio in a non-barrier structure with $d_B = 0$ nm. In this situation, the system turns into a traditional spin valve without barriers. Using such a model, our results have been validated by the theoretical works [31, 32]. Experimentally, the lateral graphene-based spin valve exhibited MR ratios of up to 10% and 9.4% in [27, 28], respectively [27, 28]. In figure 2(c), the model shows consistent results of the MR ratio in the previous experimental works. The green solid curve fits with the corresponding parameters of [27]. The simulated MR ratio of as much as 9.6% has an error of approximately 4.2% in the experimental results. The blue solid curve fits with the corresponding parameters of [28], where the simulated MR ratio of 11.7% has an error of approximately 19.7%.

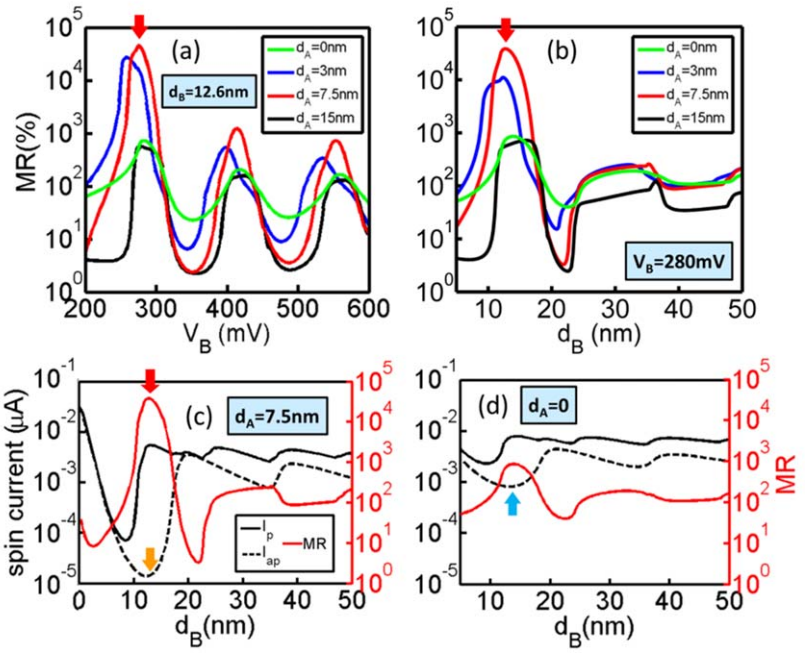

Figure 3. (a) Room-temperature MR ratio versus potential barrier V_B with fixed $d_B =$ 12.6 nm. (b) MR ratio versus thickness of each barrier d_B with $V_B =$ 280 mV. (c) Spin-polarized current and MR ratio versus thickness of each barrier d_B with fixed $d_A =$ 7.5 nm. (d) Spin-polarized current and MR ratio versus d_B with fixed $d_A =$ 0 nm. The red, yellow, and blue arrows indicate the conditions of the maximum MR. The other parameters are the same as those in figure 2.

Then, figure 3(a) shows the relationship between MR and the gated potential barrier with different distances between the two barriers. The spin polarization of the MR variation exhibits oscillatory behavior as a function of the gate voltage. The oscillation peaks are particularly high in the junction with the gate potential, where the individual resonant states are active in resonance. The maximum MR peaks are situated in the region between the gate voltages of 250 and 300 mV. Figure 3(b) shows the variations of MR with respect to the thickness of each barrier. All of the MR curves drop rapidly when d_B shifts away from 12.6 nm, and the maximum MR value appears when the thicknesses of the barrier are close to 12.6 nm. Moreover, the MR ratio shows the same order of magnitude for $d_A =$ 3 nm and $d_A =$ 7.5 nm with V_B close to 250 mV. The current features for the maximum MR ratio of $d_B =$ 12.6 nm are shown in figure 3(c). It is easy to observe a significant drop in the spin-polarized current (as indicated by the yellow arrow) in the AP configuration, corresponding to the red line in figure 3(b). In contrast to the double-barrier junctions, the situation of the current reduction is not evident when $d_A =$ 0 nm, as indicated by the blue arrow in figure 3(d) and the green curve in figure 3(b). The system turns into a traditional single-barrier spin valve. The MR ratio of approximately 850% can be attributed to the lack of an operative cavity to generate effective resonance effects in the transmission spectra (see discussion in figure 4). Furthermore, the current features are caused by the Klein tunneling [15] and the boundaries of the FG electrodes.

To understand the phenomena of current reduction and the MR value in depth, the transmission spectra in the P and AP configurations with variable barrier thicknesses are illustrated in figure 4. The red lines indicate the transmission of the maximum MR corresponding to figure 2. As shown in figure 4(a), it is clearly seen that the transmission reveals the complete and low transmission features that are caused by the resonance and the constriction in the double-barrier resonator, which can be modulated to occur in the energy ranges $[E_0 - \Delta_{ex}, E_0 + \Delta_{ex}]$ and $[E_0 + \Delta_{ex}, E_F]$, respectively. These transmissions with the barrier variation are related to both the quantum-well states formed in the central non-barrier spacer and the resonant tunneling through the entire system. These conditions are the most important to provide a significant contribution to the spin-polarized current. The discussed peaks and valleys shift with an increase in the barrier size of the junction because each spin-dependent transport has individual constriction and resonance conditions. Outside the resonance region, the transmissions are restrained under a finite barrier potential depending on the mismatch of the momentum and the length of each segment. Indeed, such a mismatch can be regulated through a combination of the momentum in the double-barrier junction. When the barrier region is set, the transmissions are suppressed drastically in addition to the resonance channel because of the strong interference from the constriction states in the central spacer, as shown in figures 4(a)–(d). Noticeably, the longitudinal momentum of the barrier has then a sign opposite to that in the other regions. The green curves present the transmission properties of the traditional graphene-based spin valves with respect to figure 2(c). The transmission restraint fails for a non-barrier case as a result of the Klein tunneling. In addition, the transmission is unable to generate

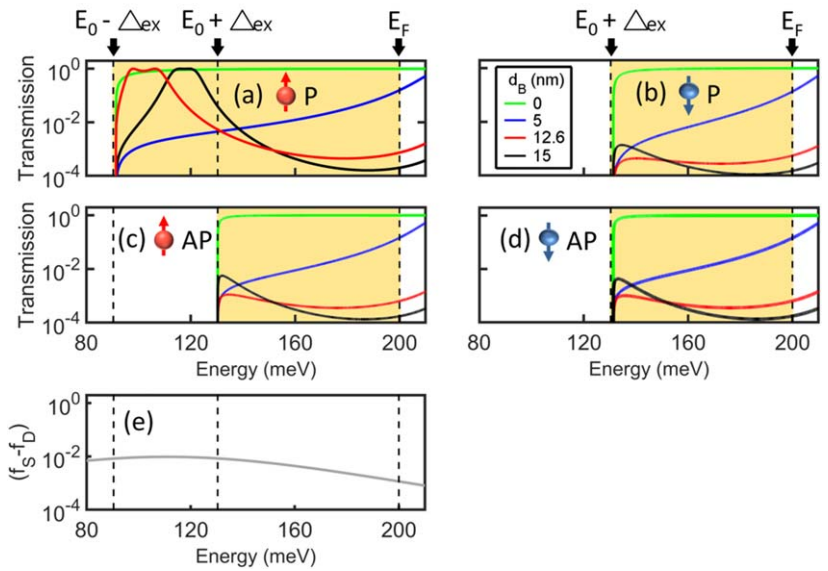

Figure 4. Transmission spectra in the P configuration of (a) spin-up and (b) spin-down electrons with different thicknesses of barrier d_B when $d_A = 7.5$ nm. Transmission of (c) spin-up and (d) spin-down electrons in the AP configuration. The red (blue) arrow represents the spin-up (spin-down) polarized electrons in the system. The energy window of the spin-polarized electrons is shaded in yellow. (e) Function of Fermi–Dirac distribution $f_S - f_D$ on the *S* and the *D* electrodes. The other parameters are the same as those in figure 2.

the constriction and the resonance if the thicknesses of the barriers are insufficient. Figure 4(e) shows the difference in the Fermi–Dirac distribution $f_S(E - \mu_S) - f_D(E - \mu_D)$. According to the current integration from equation (2), the superposition of the transmission and the Fermi–Dirac function greatly determines the magnitude of the currents. Furthermore, the peak of the Fermi–Dirac function and the resonance channel are located precisely in the energy window $[E_0 - \Delta_{ex}, E_0 + \Delta_{ex}]$ to generate a large spin-polarized current in the P configuration, as shown in figures 4(a) and (e). However, the energy states of the spin-up and spin-down electrons in the AP mode and the spin-down electrons in the P mode originate from $E_0 + \Delta_{ex}$ on the basis of the magnetization configuration and the exchange splitting of the spin. Such a resonance channel is unable to exist for the same spin-up transport owing to the AP configuration of the magnetization, as illustrated in figure 4(c). Thus, the spin-up transport contributes extremely less to the AP-mode current in the system, as seen in figure 1(c). It is found that only the transport of the spin-up polarization mainly dominates the P-mode current. Similarly, the spin-down transport is limited in both the P and AP configurations. Therefore, to further obtain higher MR ratios, it is necessary to decrease the spin-polarized current in the AP configuration. The constrictive transmissions and the lower thermal-broadening Fermi–Dirac function overlap in the entire energy window of the AP mode. The transmissions should be controlled to be considerably small in the AP configuration to generate extreme current suppression. These exceptional current features corresponding to the transmission spectra can be described by the energy states, as illustrated in figures 1(b) and (c).

This discussion explains the properties of ultra-giant MR ratio, which can be larger than that of typical spin-valve systems in this GNR-based spin valve [11, 27–29]. The number and the location of resonance channels are the main factors that greatly influence the magnitude of MR. In the present investigation, the resonance channel that appeared only between two proximity-induced splitting states generated a huge resistance difference with a change in the magnetization configuration. Such a mechanism is the characteristic for the maximum MR value with a variation of the barrier region in the junction. When the trend is correlated with the thickness increase in the central spacer, the bands of the quantum-well states between two barriers are compressed. The resonance channels can be observed in the energy window of the AP mode. It is noted that the restriction of the spin-polarized current in the AP configuration may not be able to produce the best possible effectiveness. Thus, the performance of the MR ratio is ordinary. This result is principally attributed to the larger smoothing of the Fermi–Dirac function at high temperatures. To sum up, the principal contributors to the ultra-giant MR effect are the modulation of the appropriate resonance and constriction states, causing the significant variation of the resistance in the P and AP configurations.

4. Conclusions

In conclusion, an ultra-giant MR effect at room temperature in a double gate-barrier aGNR spin valve is investigated. The result shows a huge MR ratio higher than 40 000%, which is approximately 400 times that in the graphene-based

spin valves. We found that the ultra-giant MR achieves a value approximately 60 times larger in magnitude than the MR ratio of conventional MTJ spin valves by using a strong current restriction in the AP configuration. These results are attributed to the mechanism of transmission and the Fermi–Dirac distribution, depending on the modulation of the resonance effect. The maximum MR can be observed under the condition of $d_A = 7.5$ nm, $d_B = 12.6$ nm, and $V_B = 280$ mV, where the current is drastically reduced to only a hundredth of the original value in the AP mode. However, the transport of the spin-up electrons exhibits higher transmission through the entire system in the P configuration because of the resonance. Remarkably, the MR ratio is still more than 10^4% when small variations occur in the double-barrier junction. Furthermore, given that the barriers are generated by voltage gates instead of traditional crystal insulator materials, the structure shows higher flexibility, stability, and durability. The graphene-based spin valves with the gated barriers provide an ultra-giant MR that can be applied to high-efficiency spintronics devices, including novel storage memories, read-head applications, magnetic sensors, and spin transistors.

Acknowledgments

The authors acknowledge the support provided by the Ministry of Science and Technology of Taiwan, under grant numbers MOST 106-2221-E-002-119-MY3 and MOST 105-2221-E-002-136.

ORCID iDs

Wen-Jeng Hsueh https://orcid.org/0000-0001-8542-6809

References

[1] Barnaś J and Fert A 1998 *Phys. Rev. Lett.* **80** 1058
[2] Žutić I, Fabian J and Das Sarma S 2004 *Rev. Mod. Phys.* **76** 323
[3] Fabian J, Matos-Abiague A, Ertler C, Stano P and Žutić I 2007 *Acta Phys. Slov.* **57** 565
[4] Parkin S S P, Kaiser C, Panchula A, Rice P M, Hughes B, Samant M and Yang S-H 2004 *Nat. Mater.* **3** 862
[5] Chen C H and Hsueh W J 2014 *Appl. Phys. Lett.* **104** 042405
[6] Gardelis S, Smith C G, Barnes C H W, Linfield E H and Ritchie D A 1999 *Phys. Rev.* B **60** 7764
[7] Useinov A, Lin H-H and Lai C-H 2017 *Sci. Rep.* **7** 8357
[8] Meng H, Wu J, Wu X, Ren M, Ren Y and Yao J 2018 *New J. Phys.* **20** 123024
[9] Yuasa S, Nagahama T, Fukushima A, Suzuki Y and Ando K 2004 *Nat. Mater.* **3** 868
[10] Chen C H, Cheng Y H, Ko C W and Hsueh W J 2015 *Appl. Phys. Lett.* **107** 152401
[11] Ikeda S, Hayakawa J, Ashizawa Y, Lee Y M, Miura K, Hasegawa H, Tsunoda M, Matsukura F and Ohno H 2008 *Appl. Phys. Lett.* **93** 082508
[12] Yang T, Otagiri M, Kanai H and Uehara Y 2010 *J. Magn. Magn. Mater.* **322** L53
[13] Piquemal-Banci M *et al* 2016 *Appl. Phys. Lett.* **108** 102404
[14] Dankert A *et al* 2017 *ACS Nano* **11** 6389
[15] Castro Neto A H, Guinea F, Peres N M R, Novoselov K S and Geim A K 2009 *Rev. Mod. Phys.* **81** 109
[16] Katsnelson M I, Novoselov K S and Geim A K 2006 *Nat. Phys.* **2** 620
[17] Manzoni M T, Silveiro I, Abajo F J G d and Chang D E 2015 *New J. Phys.* **17** 083031
[18] Guo G-P, Lin Z-R, Tu T, Cao G, Li X-P and Guo G-C 2009 *New J. Phys.* **11** 123005
[19] Ruffieux P *et al* 2012 *ACS Nano* **6** 6930
[20] Krompiewski S 2012 *Nanotechnology* **23** 135203
[21] Bai J, Cheng R, Xiu F, Liao L, Wang M, Shailos A, Wang K L, Huang Y and Duan X 2010 *Nat. Nanotechnol.* **5** 655
[22] Han W, Kawakami R K, Gmitra M and Fabian J 2014 *Nat. Nanotechnol.* **9** 794
[23] Zeng M, Feng Y and Liang G 2011 *Nano Lett.* **11** 1369
[24] Wang Y-T and Zhang S 2016 *New J. Phys.* **18** 113014
[25] Kim W Y and Kim K S 2008 *Nat. Nanotechnol.* **3** 408
[26] Chen C H, Chao B S and Hsueh W J 2015 *J. Phys. D: Appl. Phys.* **48** 335004
[27] Hill E W, Geim A K, Novoselov K, Schedin F and Blake P 2006 *IEEE Trans. Magn.* **42** 2694
[28] Dlubak B *et al* 2012 *Nature Phys.* **8** 557
[29] Yazyev O V and Pasquarello A 2009 *Phys. Rev.* B **80** 035408
[30] Piquemal-Banci M *et al* 2018 *ACS Nano* **12** 4712
[31] Munárriz J, Gaul C, Malyshev A V, Orellana P A, Müller C A and Domínguez-Adame F 2013 *Phys. Rev.* B **88** 155423
[32] Ferreira G J, Leuenberger M N, Loss D and Egues J C 2011 *Phys. Rev.* B **84** 125453
[33] Liu G, Velasco J, Bao W and Lau C N 2008 *Appl. Phys. Lett.* **92** 203103
[34] Barraza-Lopez S, Vanević M, Kindermann M and Chou M Y 2010 *Phys. Rev. Lett.* **104** 076807
[35] Zhang Y-T, Jiang H, Sun Q-f and Xie X C 2010 *Phys. Rev.* B **81** 165404
[36] Haugen H, Huertas-Hernando D and Brataas A 2008 *Phys. Rev.* B **77** 115406
[37] Žutić I, Matos-Abiague A, Scharf B, Dery H and Belashchenko K 2019 *Mater. Today* **22** 85
[38] Blanter Y M and Büttiker M 2000 *Phys. Rep.* **336** 1
[39] Chang C H, Tsao C W and Hsueh W J 2014 *New J. Phys.* **16** 113069